7(2010) 21 – 40

Latin American Journal of Solids and Structures

www.lajss.org

Importance of considering a material micro-failure criterion in the numerical modelling of the shot peening process applied to parabolic leaf springs

Abstract

Shot peening is a cold-working mechanical process in which a shot stream is propelled against a component surface. Its purpose is to introduce compressive residual stresses on component surfaces for increasing the fatigue resistance. This process is widely applied in springs due to the cyclical loads requirements. This paper presents a numerical modelling of shot peening process using the finite element method. The results are compared with experimental measurements of the residual stresses, obtained by the X-rays diffraction technique, in leaf springs submitted to this process. Furthermore, the results are compared with empirical and numerical correlations developed by other authors.

Keywords

shot peening, residual stresses, automotive leaf spring.

Miguel Angel Calle Gonzales[a,*], **Daniel Benítez Barrios**[b], **Nelson Batista de Lima**[c] **and Edison Gonçalves**[a]

[a] Department of Mechatronics and Mechanical Systems, Polytechnic School of the University of So Paulo, SP – Brazil
[b] Department of Mechanical Engineering, Mackenzie Presbyterian University, SP – Brazil
[c] Materials Science and Technology Centre, Nuclear and Energetic Research Institute, SP – Brazil

Received 13 Jul 2009;
In revised form 3 Dez 2009

* Author email: mcallegonzales@gmail.com

1 INTRODUCTION

The shot peening is the most widely used method to introduce compressive residual stresses on the surface of mechanical components to increase their fatigue life. Although the intense application of the shot peening process in industry for about one century, the mechanics principles of the introduction of residual stresses are not completely understood.

Only in 1995 shot peening begin to be studied scientifically when Al-Obaid [1] developed a theoretical model of the shot peening to estimate the depth of compressive residual stresses layer (DCRSL), Appendix A. This model was based on a single shot impact over a plane elastic-plastic material surface. Watanabe [21] correlated the non-dimensional parameter $\rho \cdot V_0^2 . \bar{p}^{-1}$ with the DCRSL for a more accurate solution, Appendix A.

However, due the amount of non-linearities involved in the analysis of the peening mechanism, the subsequent researches were fundamentally based on experimental and numerical analyses.

NOMENCLATURE

A, n	Material coefficients according to the Holloman model
A, B, C, n, m	Material coefficients according to the Johnson-Cook model
C, p	Strain rate sensibility coefficients according to the Cowper-Symonds model
C_p	Coverage parameter
D_d	Shot indentation diameter
D	Damage variable according the damage model of Lemaître and Chaboche model
D_c	Critic value of damage
f_Λ	Almen intensity
K	Strength material coefficient
n	Hardening coefficient
p	Accumulated plastic strain according the damage model of Lemaître and Chaboche model
$\bar{p}$	Average applied pressure (considered equal to yield strength)
R	Shot radius
T	Temperature
V_0	Initial shot velocity
Z_0	Depth of compressive residual stresses layer
ϵ	Strain
ϵ_p	Plastic strain
ε_D	Critic strain to initiate damage
ε_R	Strain at rupture when critic damage is achieved
$\dot{\varepsilon}$	Strain rate
ν	Poisson coefficient
ρ	Density
σ	Stress
σ_u	Ultimate tensile strength
σ_u^{ref}	Ultimate tensile strength of the reference material (SAE 1070 steel)
σ_y	Yield strength
σ_{eq}	Von Misses equivalent stress
σ_H	Hydrostatic stress
σ^r_{sup}	Superficial residual stress
$\sigma^r_{máx}$	Maximum compressive residual stress

ABBREVIATORS

CRSF	Compressive residual stresses field
DLCRS	Depth of layer under compressive residual stresses
MCRS	Maximum compressive residual stress
FEM	Finite elements method
SRS	Superficial residual stress

So, in 1998, Wang [20] correlated, experimentally, the residual stress field characteristics generated by shot peening with peening parameters and material mechanical properties, Appendix A. The residual stress fields were obtained from seven different materials (steels SAE 5120, SAE 4130, SAE 5140, 40CrMnSiMoVA, SAE 1045, SAE 1070 and alloy aluminum LC9) using the X-rays diffraction technique.

Similarly, Gao, Yao and Li [5] analyzed the residual stress fields of SAE 5140 steel, submitted to various heat treatments, to correlate the peening parameters with the mechanical properties. The resulting experimental correlations, Appendix A, allow giving a first estimative of the residual stress field characteristics when shot peening is applied in other steels.

In the last 10 years, promoted by the advances in computational data processing, the shot peening process began to be analyzed by the Finite Element Method (FEM). However, until now, there is not still a definitive and unique solution for the numerical modelling of this process.

Meguid, Shagal and Stranart [13] introduced a tridimensional numerical model to simulate the plastic deformation caused by two shot impacts perpendicular to a target plane surface. The model uses barely one symmetry plane. This dynamic modelling was performed using SAE 4340 steel as target material. Various peening parameters as shot velocities, shot diameters, elliptic shot shape, distances between shot impacts and plastic hardening parameters were analyzed. The elastic plastic mechanical properties of the target material and the shot as a rigid body were also considered in this research.

Guagliano [9] also developed a tridimensional numerical model with five shot impacts in a small target surface. The SAE 1070 steel was used as target material. Different shot sizes and velocities were also considered. The resultant residual stress fields were used to calculate the equivalent Almen intensity and to correlate them with their peening parameters. Moreover, this dynamic modelling utilizes two symmetric planes.

In 2002, Meguid, Shagal and Stranart [14] developed other tridimensional shot peening modelling. In this research was used a 3D cell geometry for the target material employing four symmetry planes. Furthermore, the sensibility to high strain rates in the target material was taken into account (SAE 4340 steel) using the Cowper-Symonds model, Appendix B. Thus, the significance of the strain rate sensibility in the target material behavior, during a dynamic numerical modelling of the peening process, was confirmed.

In 2004, Eltobgy, Ng and Elbestawi [3] created a 3D shot peening numerical model which take into account multiple shot impacts. Due to the evaluation of the dynamic damping effect in the modelling, it was concluded the importance of the material damping in the model.

Majzoobi, Azizi and Alavi Nia [12] simulated multiple impingements between shots and a plane surface using a 3D cell model as seen above in other research [14]. The coverage parameter was analyzed considering different number of shot impacts (from 9 to 25 shot impacts). The Johnson-Cook model (Appendix B) for the target material, SAE 4340 steel, was used. Notwithstanding the apparently uniformity of the shot indentations coverage, the difference in the residual stress values, between two points in the cell surface, achieved 40% for full coverage condition.

Frija et al. [4] implemented a tridimensional numerical modeling using the damage material model. A single shot impact in a cell geometry as target was modeled. For the target material, a nickel alloy called Waspaloy, was used the Holloman model, for the plastic behavior, and the ductile damage model proposed by Lemaître and Chaboche, Appendix B. For this material and the applied peening parameters, it was concluded that the model showed no difference when the damage model is introduced.

In 2007, Hong, Ooi and Shaw [10] created a single shot impact 3D modelling. A dimensionless analysis to evaluate the influence of the shot size, shot velocity, hardening coefficient, yield strength and impact angle on the residual stress field was used. These analyses [9] demonstrated that all these parameters has a significant influence in the generation of the residual stress fields. Furthermore, the dimensionless analysis made able these results to be applied to other materials.

Here, a numerical modelling of the shot peening process applied to leaf springs was developed using the FEM. The numerical models are based on explicit formulation, which takes into account tridimensional modelling of multiple shot impacts, real shot velocity estimation and friction between contact surfaces. A 3D cell numerical model to represent the peened surface, as used in Refs. [12, 13], were not considered because the displacement constraints effects are significant since the size of the cell and the shot diameter are the same, Ref. [7]. All the reviewed researches about peening modellings estimate the shot velocity based on theoretical relationships of this shot velocity with the Almen intensity estimated by other authors, Ref. [9], otherwise the source of the shot velocity is not mentioned.

In this work, the real shot velocity is calculated based in the geometry of the peening machine and the kinematics of a shot when it travels through the peening wheel blade. Moreover, the elastic-plastic mechanical properties and its sensitivity to high strain rates were considered because their relevance in the numerical results, Ref. [14].

Furthermore, this works presents a new method to evaluate a representative CRSF by averaging all the CRSF, along the depth, for all the nodes affected by the shot indentations in the treated area. This method is presented as a replacement of evaluating the CRSF punctually in a node, along the depth, as carried out by all the reviewed researches about peening modellings, Ref. [3, 4, 9, 10, 12–14].

An experimental programme for evaluation of the residual stresses using the X-ray diffraction technique in the parabolic leaf springs was also performed and described here.

2 PARABOLIC LEAF SPRINGS

The parabolic leaf spring analyzed in this work is a component of the transversal suspension system of the front axle of a van. The thickness of the parabolic leaf spring is larger in the middle than in the extremes. This geometry provides a better use of the material when submitted to the service bending loads. The material of the leaf spring is the SAE 5160 steel, which was developed specifically for the automotive springs manufacturing. Table 1 lists the main chemical components of this steel.

Table 1 Chemical composition of the SAE 5160 steel.

Carbon	Manganese	Silicon	Chrome	Vanadium	Molybdenum
0.56 to 0.64%	0.75 to 1%	0.15 to 0.3%	0.7 to 0.9%	0.15%	0.15 to 0.25%

The manufacture process of a parabolic leaf spring begins with the generation of the geometry, application of the heat treatments (quenching from 840 °C in oil and tempering at 450 °C for 10 h), application of the peening process, cleaning, painting and quality control. The mechanical properties (Table 2) were obtained from standard tensile tests using an Instron model 3369, see Fig. 1.

Table 2 Mechanical properties of the SAE 5160 steel.

Modulus of elasticity	185 GPa
Poisson coefficient	0.3
Yield strength	1240 MPa
Ultimate tensile strength	1360 MPa
Rupture strength	1318 MPa
Area reduction	16.9%
Hardness	39.2 HRc
Density	7740kg/m^3

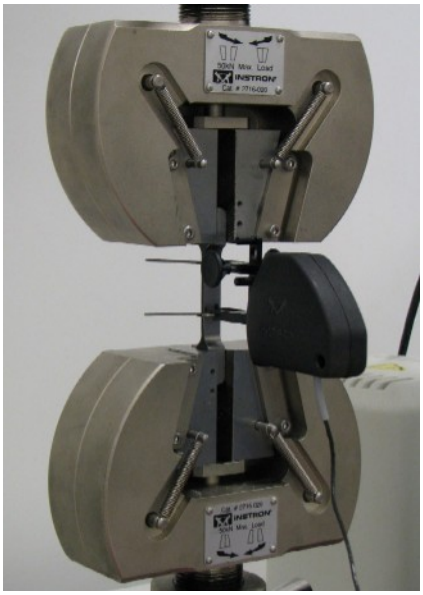

Figure 1 Tensile test of the SAE 5160 steel and detail of the clip gage instrumentation.

The Almen intensity applied to the springs in the shot peening processes was 0.92 mm (Almen strip A) and the shot size was S330. The Almen intensity measurement methodology and shot size specifications are established by the SAE standards and specified in the catalog of the shot manufacturer, Ref. [17, 18]. The shots used are fabricated in steel with martensitic structure (from 0.8 to 1.2% carbon, from 0.6 to 1.2% magnesium and 0.4% silicon) with hardness, of at least 80% of the shots, between 47 and 54 HRc.

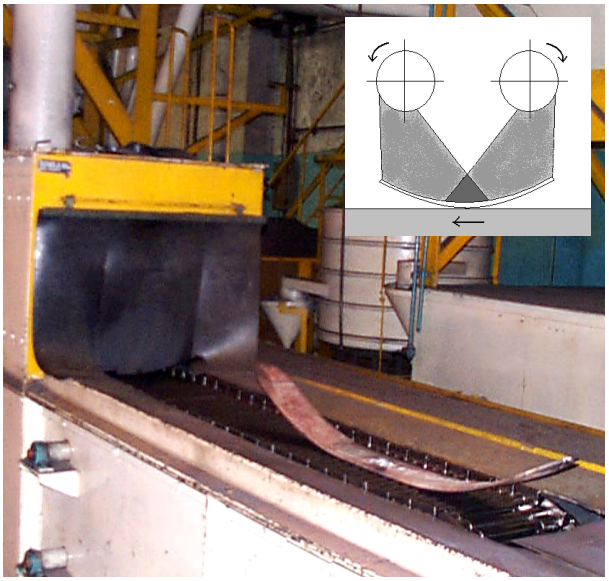

Figure 2 Leaf springs submitted to the shot peening process.

3 EXPERIMENTAL MEASUREMENT OF THE RESIDUAL STRESS FIELD

The experimental measurement of the residual stress fields in the leaf springs submitted to the shot peening processes was developed using the X-rays diffraction. Eleven specimens were extracted from the parabolic leaf spring submitted to the peening process, Fig. 3. Also, one specimen was extracted from one spring not submitted to the peening process (AΩ) to analyze the initial residual stresses before the application of this process.

The residual stresses measurements using the X-ray diffraction technique were developed on a Rigaku diffractometer, model Demax, Fig. 4a. The method used was $\mathrm{Sin}^2\ \psi$ using 13 readings (covering from -60° to 60°) irradiating Cr Kα at the crystallographic lattices (2 1 1). Since the X-ray diffraction technique is only capable to measure the superficial stress of a specimen, for obtaining the residual stresses field along the depth of the specimen, thin layers of material were sequentially removed by chemical etching using nitric acid diluted in water, Figure 4b. Given that the thickness of the removed layer of material depends of the time and temperature of the chemical etching as well as the hardness of the revealed surface, the thickness of the removed layer of material is not the same in every step.

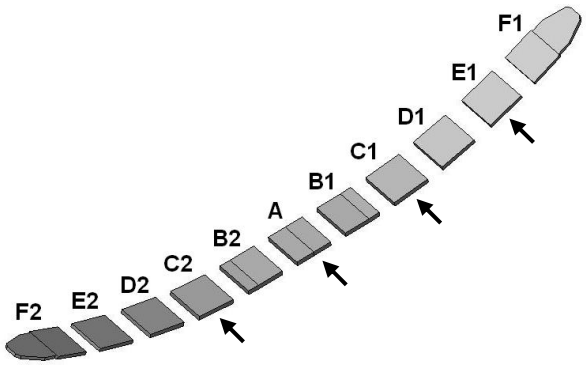

Figure 3 Specimens from the leaf springs submitted to the shot peening.

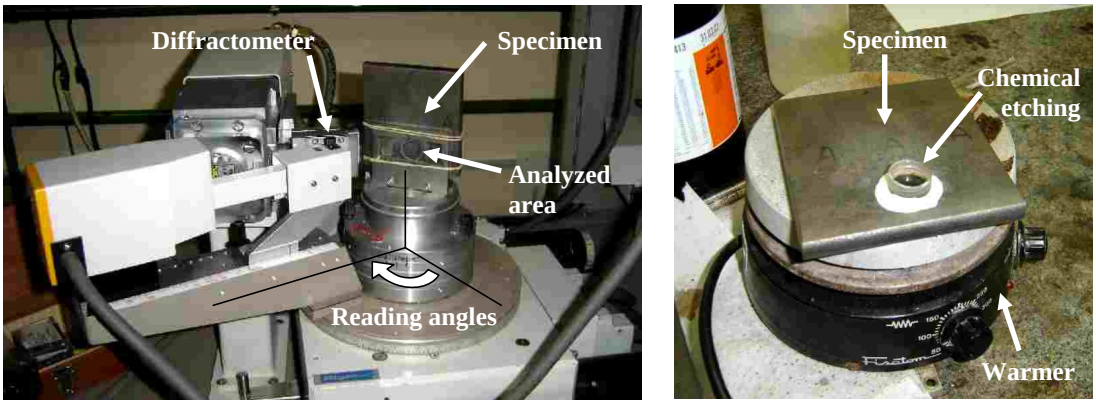

(a) (b)

Figure 4 Measurement of the residual stresses fields in the leaf springs specimens using a) X-rays diffraction technique and b) chemical etching.

The residual stresses fields in the z direction (along the longitudinal direction of the leaf spring) so measured were obtained for the specimens A, C1, C2 and E1 as shown in Fig. 5.

The specimen AΩ showed nearly constant values of residual stresses of 28 ± 10 MPa until 150 μm depth. Due the small residual stress values (small when compared with the residual stresses induced by a peening process), the source material can be considered without residual stresses.

4 NUMERICAL AND COMPUTATIONAL MODELLING OF THE SHOT PEENING PROCESS

In order to explore further the effects of shot peening on the leaf material properties, a numerical modelling of the shot peening process based on the finite element method was carried out. The spring mechanical properties as well as the experimental peening parameters were used as reference to develop the numerical models.

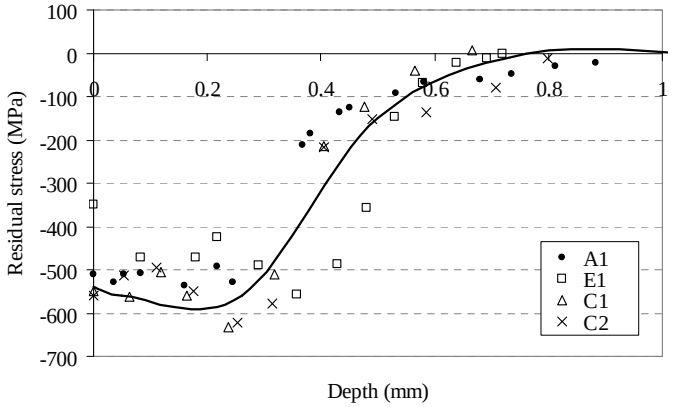

Figure 5 Residual stresses fields obtained using the X-rays diffraction technique for the specimens submitted to the shot peening process.

The material model used to represent the leaf spring steel is multilinear elastic-plastic, isotropic and strain rate sensitive, as implemented in the LS-DYNA code. This material model uses the Cowper-Symonds formulation for correcting the quasi-static stress-strain curve, for high strain rates where $C = 120000\ \mathrm{s}^{-1}$ and $p = 3.9$ [6]. The shots were considered rigid since their hardness is much greater than the leaf spring steel, see Table 2.

In the peening process, the peening intensity is directly related to the average shot velocity, Ref. [9]. For this reason, the estimative of the real shot velocity is important for the numerical modelling. The peening machine uses a rotational wheel with blades to impel the shots, Fig. 6a. The shot velocity, when the shots reach the wheel periphery, is composed by tangential and radial components, Fig 6b. The tangential and radial components of the shot velocities are calculated based on simplified kinematics formulations, which takes into account the peening wheel characteristics, Table 3.

Table 3 Characteristics of the shot peening machine.

Wheel diameter	440 mm
Wheel speed	1450 rpm
Motor power	75 cv
Blade length / wheel radius	0.6
Motor speed	1750 rpm
Number of wheels	2
Assembly of the wheels	series

The shot velocity is achieved in two stages. In the first stage, the shots are centrally fed in the wheel into a control cage and accelerated by the centrifugal forces but restrained by the control cage. Subsequently, in the second stage, the shots escape from the control cage by an outlet slot and continue to be accelerated, but without restraints, by the wheel blades.

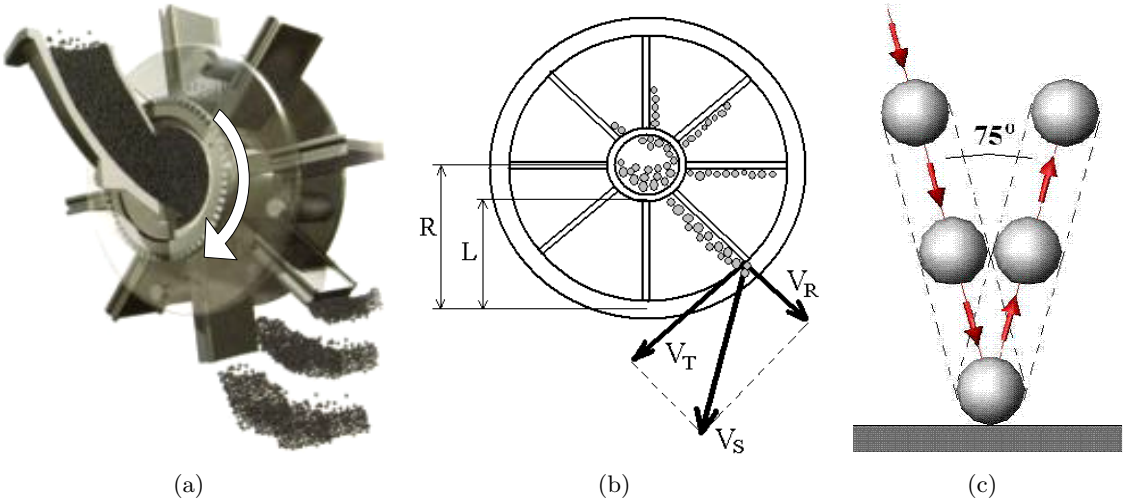

Figure 6 a) Shots impelled by the peening wheel, b) Shot velocity components when shots reach the wheel periphery and c) rebounding shot angle to let free flux.

The slipping of the shot through the surface of the blade is considered without rebounding, spinning, friction or interference with other shots. Thus, the final velocity of one shot can be estimated when the shot detaches the wheel periphery. If N is the wheel rotational velocity, the tangential component can be calculated directly by $v_t = xN$ where v_t is the tangential velocity of the shot media for a radial position x measured from the center of the wheel, passing through the control cage outlet and along slipping the blade surface. When the shot leaves the wheel, it achieves the higher tangential velocity $V_T = RN$, where R is the radius of the wheel.

When the shot leaves the control cage, the tangential velocity, induced by the rotating blade, generates a centrifugal acceleration on this shot given by $a_c = \frac{v_t^2}{x} = xN^2$. From the well known relationships for acceleration and velocity in the radial direction, $a_c = \frac{dv_r}{dt}$ and $v_r = \frac{dx}{dt}$, is obtained the relationship $v_r dv_r = a_c dx$ which can be described also as $v_r dv_r = N^2 x dx$.

Integrating both terms of equation from the control cage outlet to the perimeter of the wheel, $\int_0^{V_R} v_r dv_r = N^2 \int_{R-L}^{R} x dx$, the final radial velocity ca be found $V_R = N\sqrt{2RL - L^2}$.

Then, the total velocity becomes the resultant of the tangential and radial components $V_S = \sqrt{V_T^2 + V_R^2}$. The radial component of this equation is corrected by the factor 0.8 due to the friction between the shot media and the blade surface, Ref. [11], and replacing $L/R = 0.6$, results $V_S = \sqrt{V_T^2 + (0.8V_R)^2} = 1.24NR$.

Finally, the final shot velocity is considered as the vertical component when the shot collides the surface in an angle $\alpha°$. The α angle is the minimum angle which lets free flux of a shot stream to impact a plane surface (75°) so the correction factor applied to the final velocity is $\sin(\alpha) = \sin(75°) = 0.966$, Fig. 6c.

By so proceeding, the shot velocity was estimated in 40.01 m/s.

The numerical model geometry of the shot peening process is composed by a restrained

flat plate, which represents the surface of the treated leaf spring, and 30 rigid spheres, which represent the shots colliding against the leaf spring surface. The impacts between the rigid spheres and the flat plate are perpendicular, Fig. 7. The velocity for all the shots was defined in 40.01 m/s.

The shot size used was the S330 whose distribution by quantity, extracted from the distribution by weight, Ref. [18], was distributed in only 7 shot sizes, Fig. 8. Only the bigger shot sizes, from 0.925 to 1.29 mm shot diameter were considered, because the smaller shots are merely used to achieve full coverage faster, Ref. [11]. Multiple shot impacts were implemented in the numerical model following this shot size distribution.

Only a small target area of the flat plate (1 mm diameter) was submitted to the rigid spheres impacts, see Fig. 7. This ensures that the displacement boundary conditions, set along all the flat plate edge, do not interfere with the generation of the residual stresses fields during the shot impacts application. This small area of the numerical model represents, on a small scale, what happens in the real process when a surface is submitted to the shot peening [10, 12, 13].

Only half of the plate was modeled. The plate is circular, with an outer diameter of 5 mm and thickness of 2.5 mm. The plate is restrained in the symmetry plane around its edge and in its bottom. The target locations of the shot impacts and shot sizes are shown in Fig. 7.

5 EVALUATION OF THE AVERAGE RESIDUAL STRESSES FIELD

The compressive residual stresses fields (CRSF) were evaluated in the points V, F, A, H, L and W. This analysis demonstrates that the residual stresses can not be analyzed only from one point of the surface and along the depth because a difference between the stresses of one field and another, depending of the position of the point in the surface for the same depth, can achieve 200%. For instance, the points A and H show a difference of 60% when the superficial residual stresses (SRS) were compared, Fig. 9. Another important point to note is the significant difference between the CRSF, induced for the same point, but in the x and z directions. So, the point A show a difference of 75% when the SRS in both directions, x and z, were compared, Fig. 9.

The small target area was divided in 5 subareas in the form of concentric rings ($\Lambda 1$, $\Lambda 2$, $\Lambda 3$, $\Lambda 4$ and $\Lambda 5$) with outer diameters of 0.1, 0.2, 0.3, 0.4 and 0.5 mm respectively, Fig. 10.

Figure 11 shows the average residual stresses fields in x and z directions induced by the shot peening process for the various subareas and along the depth y direction. This analysis was performed after the 30 shots impacts in the case of the shot peening modelling.

Due to the poor penetration detected at points V, W and L, both in subarea $\Lambda 5$, the representative areas, considered for the estimative of the average residual stresses fields induced in the numerical modelling only take into account the subareas $\Lambda 1$, $\Lambda 2$, $\Lambda 3$ e $\Lambda 4$, Fig. 10.

It can be seen in Figure 11 typical residual stresses field induced by the shot peening process. A layer with compressive residual stresses begins in the surface and the compressive value increases along the depth up to a maximal value, decreasing till it turns to a tensile

Impact	Shot diameter (mm)	Target position
1st	1.290	A
2nd	1.090	B
3rd	1.090	E
4th	1.090	C
5th	1.090	A
6th	1.090	D
7th	1.090	B
8th	1.090	H
9th	0.925	C
10th	0.925	D
11th	0.925	A
12th	0.925	K
13th	0.925	F
14th	0.925	G
15th	0.925	D
16th	1.290	A
17th	1.090	B
18th	0.925	E
19th	1.090	C
20th	0.925	A
21st	0.925	D
22nd	1.090	B
23rd	0.925	E
24th	1.090	C
25th	0.925	I
26th	0.925	A
27th	0.925	E
28th	0.925	F
29th	0.925	G
30th	0.925	J

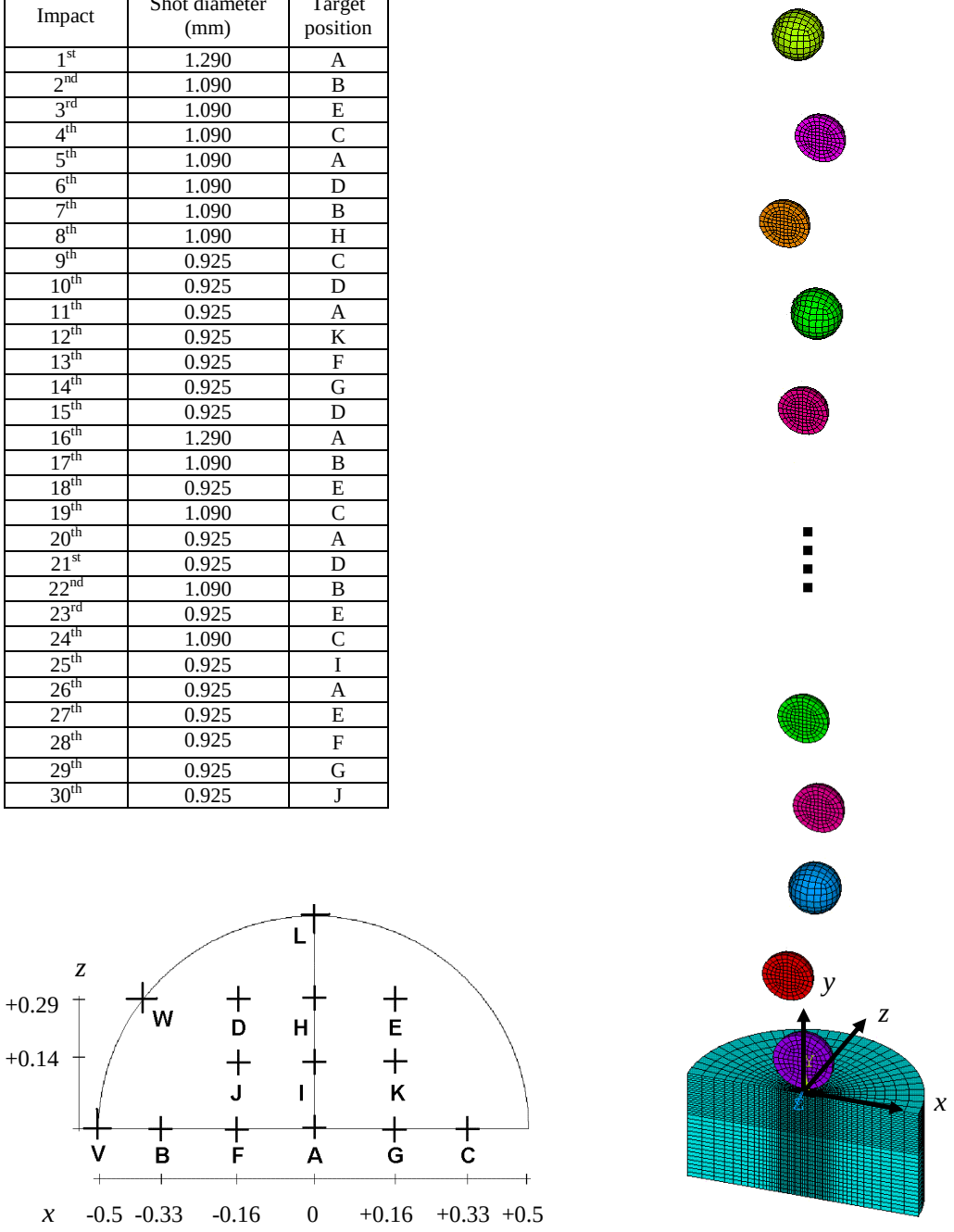

Figure 7 Geometry of the numerical model and positions of the 30 shot impacts in the small target area of the flat plate.

value. Can be seen also that there is a perceptible difference between the compressive residual stresses fields (CRSF) depending of the analyzed subarea. Taking into account only the valid

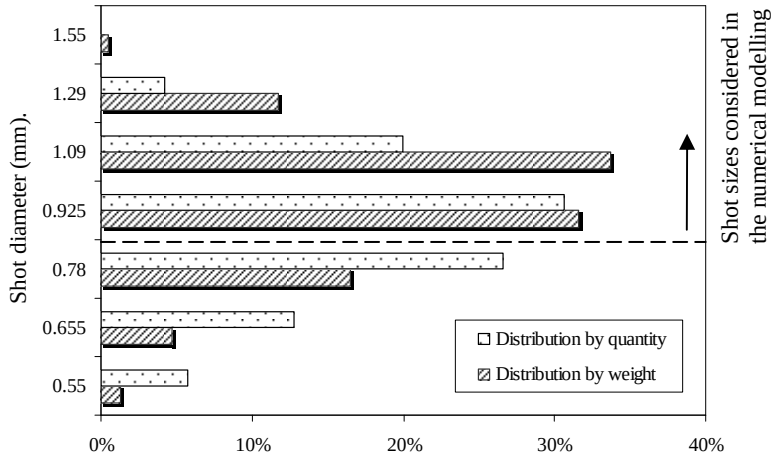

Figure 8 Distributions of the shots by quantity and individual weight.

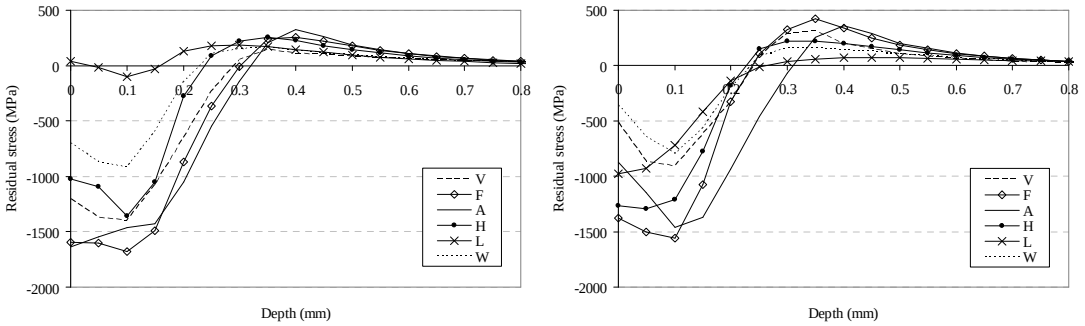

Figure 9 Residual stresses fields in x and z directions obtained for specific points.

subareas (from $\Lambda 1$ to $\Lambda 4$), the CRSF induced in the x direction showed a maximum difference of 80% for the superficial residual stress (SRS), 20% for the maximum compressive residual stress (MCRS) and 25% for the depth of layer under compressive residual stresses (DLCRS).

Therefore, the calculation of an average CRSF over an area submitted to shot peening is more representative than an analysis considering only a point of the same area due to the observed differences, presented in the CRSF, for every individual subarea.

Figure 11 also shows that the average residual stresses fields induced in the x and z directions are nearly the same. For this reason, these fields are considered identical.

6 COMPARATIVE ANALYSIS

The numerical results of the shot peening process is compared with theoretical results and empirical correlations in Ref. [1, 5, 20, 21], Fig. 12a, and with correlations obtained by numerical modellings developed by other authors in Ref. [10, 13, 14], Fig. 12b.

Figure 12 shows that the magnitudes of SRS and MCRS, obtained in the numerical modelling, are higher than the experimental measurements by 60% and 100%, respectively, and that

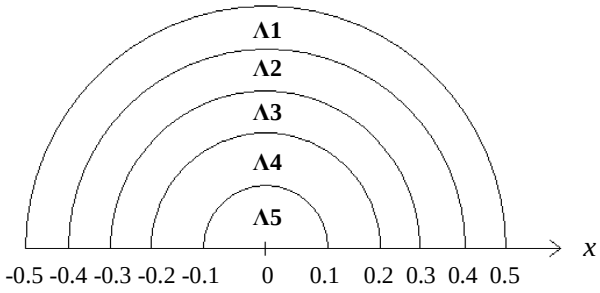

$$\Lambda = \Lambda 1 + \Lambda 2 + \Lambda 3 + \Lambda 4$$

Figure 10 Small target area division for residual stresses analysis.

the DLCRS is lower by almost 50%. Both phenomena have also been observed in correlations obtained by numerical modellings developed by other authors, Refs. [10, 13, 14].

7 DISCUSSION OF THE RESULTS

The amount of deformation energy is defined as the elastic and plastic energy absorbed per area by the leaf spring surface due to the shot peening application. This energy is estimated by the integral of the compressive residual stresses along the depth, Fig. 13a. The evaluation of this integral is also important for the analysis of the flexure moment produced by the CRSF in an Almen strip, Refs. [9, 16], or the curvature induced in a plate submitted to the peen forming process, Ref. [2].

The deformation energy estimated for the CRSF obtained experimentally is similar to the one yielded by the numerical model, Fig 13b. The deformation energy for the residual stresses field induced in the numerical modelling results -243.5 MPa.mm. The error of the deformation energy induced by the numerical modelling when compared with the deformation energy of the specimens C2, A, C1 and E1, obtained from the experimental measurements, are 5.05, 13.1, 4.94 and 0.95% respectively, Fig. 13b.

A common aspect in the numerical modelling of the shot peening developed in the literature is the lack of an implementation of a failure criterion for peened material. The plastic deformation induced in a peened surface is not the same as the induced by a monotonic load, surfaces submitted to the shot peening process are subjected to cyclic hardening and cyclic softening which reduce the mechanical resistance of the material similarly as a strain fatigue test, Ref. [15]. Other phenomenon observed in the surfaces of specimens submitted to the shot peening process is the generation of micro-fissures close to the area of the indentations generated by the shot impacts, Ref. [8].

These phenomena may explain the difference between the numerical and the experimental DLCRS results. The reduction of the mechanical resistance of the treated material and the generation of the micro-fissures weaken the exposed upper layers of the material, so allowing a greater penetration of the shot impacts which, in turn may cause a deeper distribution of the residual stresses along the lower layers of the depth.

In Figures 14 and 15 is presented the evolution of the stresses fields along depth for the

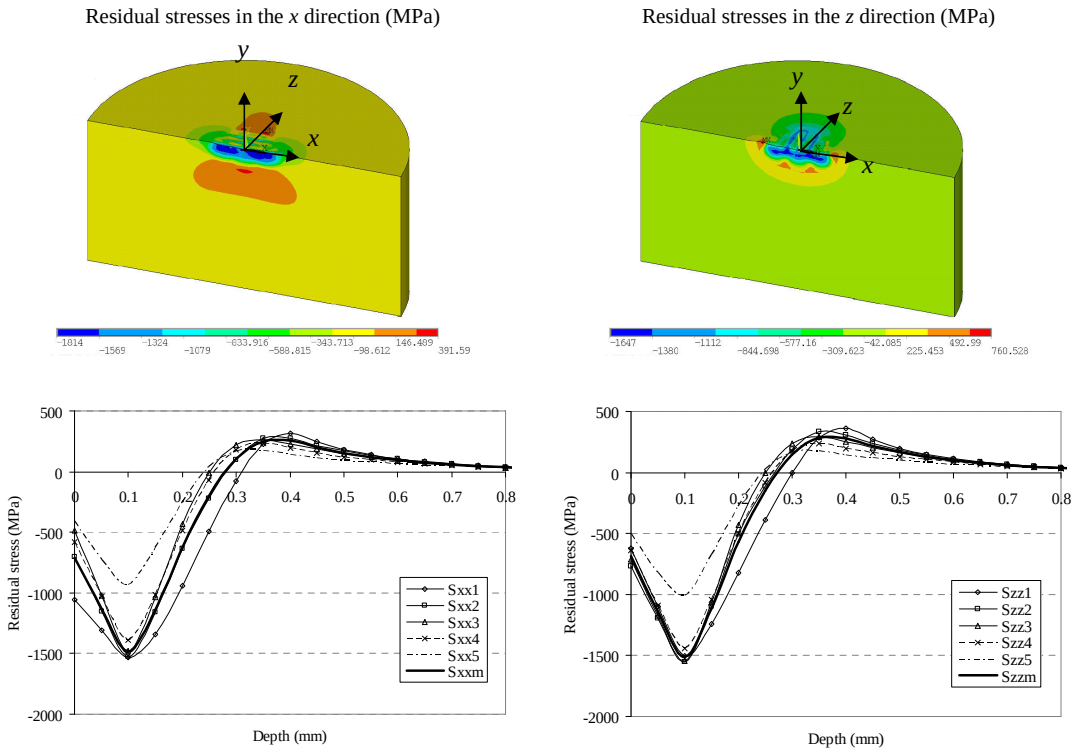

Figure 11 Residual stresses fields in x and z directions obtained from the shot peening modelling.

point A during the first and the fifth shot impacts, both impacts also targeted in this point. In Figure 16 can be seen that, during the first impact, the DLCRS increases till the value of 0.3 mm. However this value does not increase anymore during the fifth shot impact because the plastic compressed upper layers act as a resistant layer which avoids the progressive penetration of the shot impact along depth allowing only further elastic deformation.

On the other hand, the work by Frija et al. [4] discusses the implementation of a damage model for a nickel alloy called as Waspaloy in the shot peening modelling. For this material, Frija et al. [4] demonstrated that the introduction of damage did not affect significantly the resulting CRSF without considering it. However, this conclusion can not be extended to other materials because the majority of the numerical modellings of the shot peening process reviewed in the literature [10, 12, 14], only consider the SAE 4340 as the target material which shows high mechanical resistance and absence of inner micro-failure of the upper layers of the surface submitted to the shot impacts, Ref. [19].

8 VALIDATION OF THE NUMERICAL MODELLING METHODOLOGY

The numerical modelling of the SAE 4340 steel when submitted to the shot peening process, using the same methodology used for the SAE 5160, was also developed in this work. The same geometry, except for adjusting the shot size to the S230 size, as well as the same contact

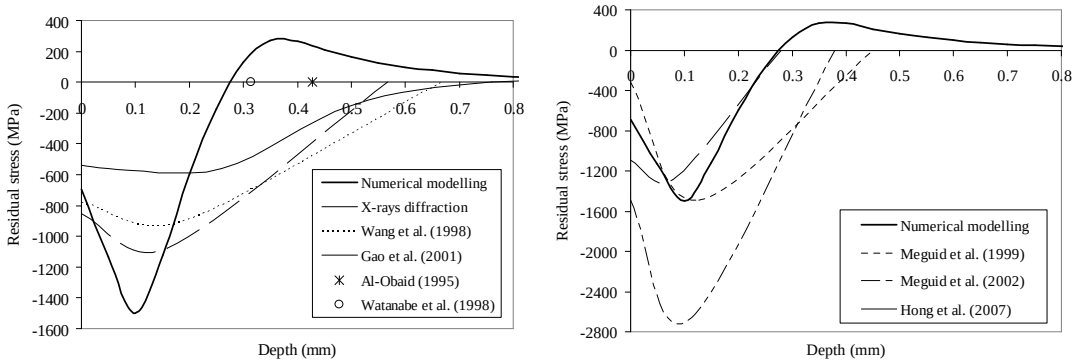

(a) (b)

Figure 12 Comparison of residual stresses fields obtained by the numerical modelling of the shot peening process with a) the experimental measurements and with b) numerical modellings of other authors.

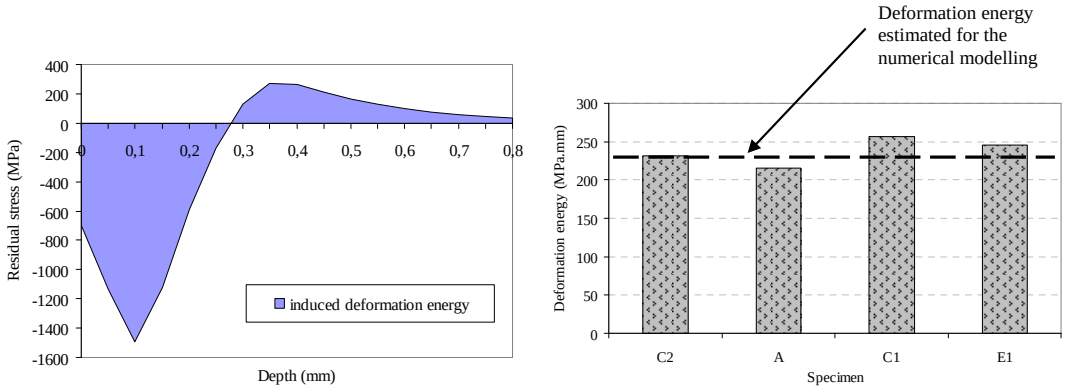

(a) (b)

Figure 13 Deformation energy of the numerical modelling compared with the estimated experimentally for the specimens C2, A, C1 and E1.

constraints, evaluation of the residual stresses field average and the elastic-plastic mechanical properties of the SAE 4340 steel were also considered. The mechanical properties considered in the numerical modelling are density of 7800 kg/m^3, elastic modulus of 210 GPa, poisson ratio of 0.3, yield limit of 1500 MPa, plastic modulus of 1600 MPa and the Cowper-Symond coefficients of $c = 200000$ and $p = 3.3$. The perpendicular shot velocity was adjusted to 50 m/s.

Similarly as the SAE 5160 steel shot peening modelling, a failure criterion for the material was not used. Nevertheless this fact, the numerical modelling results correspond with the experimental measurement of the CRSF, Ref. [19], closer than the numerical results of other author in which the CRSF was obtained along the depth from barely one point in the surface, Ref. [12], Fig. 17.

In these results can be observed that, in view of the fact that the target materials do

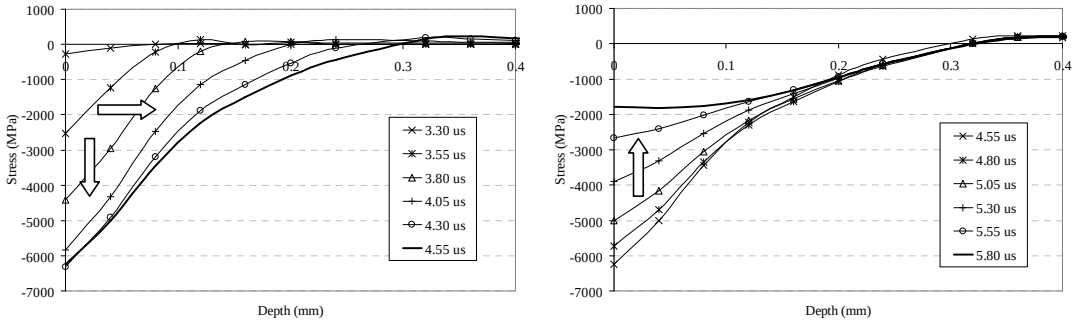

Figure 14 Evolution of the stresses field in the x direction at the point A during first shot impact.

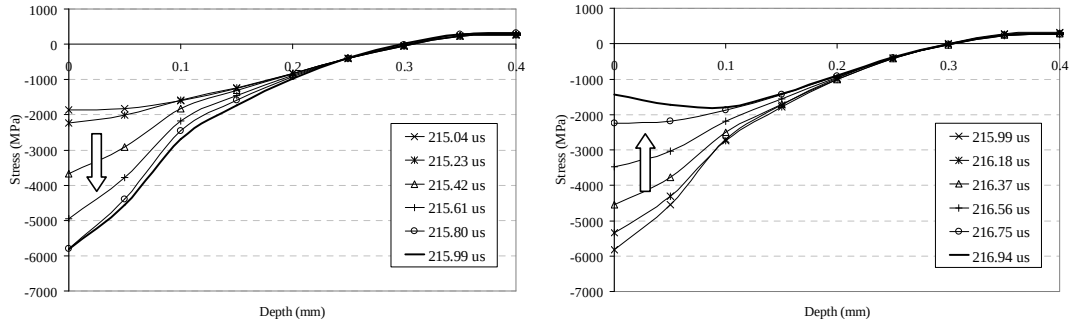

Figure 15 Evolution of the stresses field in the x direction at the point A during fifth shot impact.

not show any kind of predisposition to generate inner micro-failure or degradation of the mechanical properties of the material (for the imposed peening conditions), the integral CRSF is attained, just after the first shot impact, and this CRSF is not affected for further upcoming shot impacts as the same way as the numerical modelling of the SAE 5160.

9 CONCLUSIONS

The main conclusions inferred from this study are:

1. A unique numerical modelling for the shot peening process can not be used for all the materials because, in some cases, as when employed the SAE 5160 steel, it will be necessary to introduce a damage or micro-failure criterion to represent the weakness of the mechanical properties of the material after successive shot impacts.

2. The shot peening modelling developed here showed to be consistent with the results by other authors for similar conditions;

3. The multiple shots impacts, considered on the numerical models, represented more faithfully the real peening processes. Also, the evaluation of the average residual stresses fields, considering all the nodes of the entire treated area in the numerical modelling resulted to be more significant than the evaluation in only one central line;

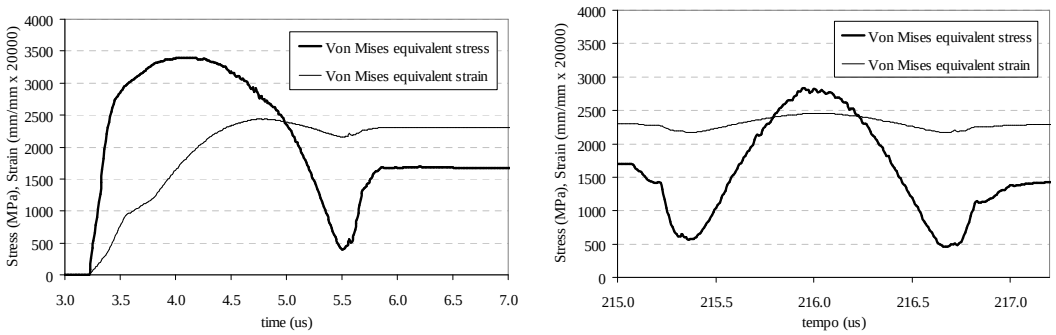

Figure 16 Evolution of the equivalent stress and strain at the point A during the first and fifth shot impacts.

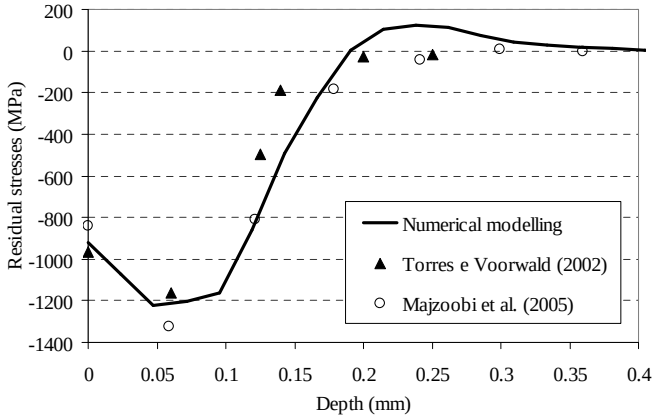

Figure 17 Comparison between the CRSF obtained by numerical modelling of shot peening and the experimental results obtained by Torres and Voorwald [19].

References

[1] Y. F. Al-Obaid. Shot-peening mechanics: Experimental and teorical analysis. *Mechanics of Materials*, 19:251–260, 1995.

[2] D.B. Benítez, M.A.C. Gonzales, A.H.P. Andrade, N.B. Lima, and E. Gonçalves. Theoretical principles of peen forming: An experimental and numerical analysis. In *Proceedings of the 19th International Congress of Mechanical Engineering, 19th COBEM*, Brasilia, Brazil, 2007.

[3] M.S. Eltobgy, E. Ng, and M.A. Elbestawi. Three-dimensional elastoplastic finite element model for residual stresses in the shot peening process. In *Proceedings of the Institution of Mechanical Engineers, Part B: Journal of Engineering Manufacture*, volume 218, pages 1471–1481, 2004.

[4] M. Frija, T. Hassine, R. Fathallah, C. Bouraoui, and A. Dogui. Finite element modeling of shot peening process: Prediction of the compressive residual stresses, the plastic deformations and the surface integrity. *Materials Science and Engineering A*, 426:173–180, 2006.

[5] Y-K. Gao, M. Yao, and J-K. Li. An analysis of residual stress fields caused by shot peening. *Metallurgical and Materials Transactions A*, 33A:1775–1778, 2002.

[6] M.A.C. Gonzales. Numerical and experimental analysis of the residual stresses induced by shot peening in automotive springs, doctoral thesis in mechanical engineering. Technical report, Polytechnic School of the University of Sao Paulo, 2009. In portuguese.

[7] M.A.C. Gonzales, D. B. Benítez, E. Gonçalves, and E. Angelo. Numerical modelling of the shot peening process using a representative 3D cell. In *Proceedings of the 7th Symposium on Computational Mechanics, 7th SIMMEC*, Minas Gerais, Brazil, 2006. In portuguese.

[8] M.A.C. Gonzales and I. Machado. Shot-peening processing effects in the microstructure and mechanical properties of a SAE 1070 steel. In *Proceedings of the 2th Brazilian Congress of Manufacturing Engineering, 2nd COBEF*, Uberlndia, Brazil, 2003. In portuguese.

[9] M. Guagliano. Relating almen intensity to residual stresses induced by shot-peening: A numerical approach. *Journal of Materials Processing Technology*, 110:277–286, 2001.

[10] T. Hong, J.Y. Ooi, and B.A. Shaw. A numerical study of the residual stress pattern from single shot impacting on the metallic component. *Advances in Engineering Software*, 39(9):743–756, 2007.

[11] D. Kirk. Generation of wheel-blast shot velocity. the shot peener. *Electronics Incorporated*, 21(2):24–30, 2007.

[12] G.H. Majzoobi, R. Azizi, and A. Alavi Nia. A three-dimensional simulation of shot peening process using multiple shot impacts. *Journal of Materials Processing Technology*, 164-165:1226–1234, 2005.

[13] S.A. Meguid, G. Shagal, and J.C. Stranart. Finite elements modeling of shotpeening residual stresses. *Journal of Materials Processing Technology*, 92-93:401–404, 1999.

[14] S.A. Meguid, G. Shagal, and J.C. Stranart. 3D finite elements analysis of peening of strain-rate sensitivity materials assign multiple impingement model. *International Journal of Impact Engineering*, 27:119–134, 2002.

[15] W. Renzhi, L. Xiangbin, T. Yonggui, and Y. Minggao. Investigation on the microstructure in shot-peening surface straining layer of materials. In *Proceedings of the international conference of shot peening*, pages 185–192, 1981.

[16] G.M. Rybakov. Energy saturation of metal parts in surface plastic deformation (shot peening). *Russian Engineering Research*, 28(11):112–114, 2008.

[17] SAE J442. Test strip, holder, and gage for shot peening. *International Society of Automotive Engineers. SAE Standards*, 2006.

[18] SAE J444. Cast shot and grit size specifications for peening and cleaning. *International Society of Automotive Engineers. SAE Standards*, 1993.

[19] M.A.S. Torres and H.J.C. Voorwald. An evaluation of shot peening, residual stress and stress relaxation on the fatigue life of AISI 4340 steel. *International Journal of Fatigue*, 24:877–886, 2002.

[20] S. Wang, Y. Li, M. Yao, and Wang R. Compressive residual stress introduced by shot peening. *Journal of Materials Processing Technology*, 73:64–73, 1998.

[21] Y. Watanabe and N. Hasegawa. Simulation of residual stress distribution on shot peening. In *Proceedings of the 6th International Conference of Shot Peening, n. 037*, San Francisco, CA, United States, 1996.

APPENDIX A

Theoretical and experimental formulations to calculate the residual stress fields characteristics generated by shot peening process

Theoretical formulation by Al-Obaid (1995) [1]

$$\frac{Z_0}{R} = 3 \cdot \left(\frac{2}{3}\right)^{1/4} \cdot \left(\frac{\rho \cdot V_0^2}{\bar{p}}\right)^{1/4}$$

Theoretical correlation by Watanabe and Hasegawa (1996) [21]

$$\frac{Z_0}{R} = 24,68\left(\frac{\rho \cdot V_0^2}{\bar{p}}\right)^{3/4} - 16,0\left(\frac{\rho \cdot V_0^2}{\bar{p}}\right)^{2/4} + 4,58\left(\frac{\rho \cdot V_0^2}{\bar{p}}\right)^{1/4}$$

Experimental correlations by Wang et al. (1998) [20]

$$Z_0 = 0,04 + \left(1,392 + 0,611\left(\frac{\sigma_u}{\sigma_u^{ref}}\right)\right) f_\Lambda \qquad (mm)$$

$$\sigma^r_{\text{sup}} = 120 + 0,5\sigma_y \qquad (MPa)$$

$$\sigma^r_{máx} = \begin{cases} 70 + 0,667\sigma_u & (\text{MPa}) \text{ for } \sigma_\text{u} < 1000 \text{ MPa} \\ 430 + 0,323\sigma_u & (\text{MPa}) \text{ for } \sigma_\text{u} \geq 1000 \text{ MPa} \end{cases}$$

Experimental correlations by Gao, Yao and Li (2002) [5]

$$Z_0 = (1,41D_d - 0,09S)\left[1 + 0,09\left(C_p - 1\right)^{0,55}\right] \qquad (mm)$$

$$\sigma^r_{\text{sup}} = 0,997\left(114 + 0,563\sigma_y\right)(MPa)$$

$$\sigma^r_{máx} = 0,86\sigma_y - 51(MPa)$$

APPENDIX B

Material models

Model proposed by Cowper-Symonds

$$\sigma = K\varepsilon^n \left[1 + \left(\frac{\dot{\varepsilon}}{C}\right)^{\frac{1}{p}}\right]$$

Model proposed by Johnson-Cook

$$\sigma = (A + B\varepsilon^n)(1 + C\ln\dot{\varepsilon})(1 - T^m)$$

Model proposed by Holloman

$$\sigma = A\varepsilon_p^n$$

Ductile damage model proposed by Lemaître and Chaboche

$$D \cong \frac{D_c}{\varepsilon_R - \varepsilon_D}\left(p\left[\frac{2}{3}(1+\nu) + 3(1-2\nu)\left(\frac{\sigma_H}{\sigma_{eq}}\right)^2\right] - \varepsilon_D\right)$$